npj | flexible electronics

www.nature.com/npjflexelectron

ARTICLE OPEN

Check for updates

Fibrillary gelation and dedoping of PEDOT:PSS fibers for interdigitated organic electrochemical transistors and circuits

Young Jin Jo[1], Soo Young Kim[1], Jeong Hun Hyun[1], Byeonghak Park[1], Seunghwan Choy[1], Gyan Raj Koirala[1] and Tae-il Kim[1,2]✉

As one of conducting polymers, PEDOT:PSS, is commonly used in organic electronics, especially for bioelectronics due to its advantages such as high electrical and ionic conductivity, solution-processability and biocompatibility. Creating bioelectronics with the PEDOT:PSS requires advanced techniques to obtain physical/chemical modification of the PEDOT:PSS for improved performance and various applications. To satisfy these demands, fibrillary gelation of PEDOT:PSS by injection to choline acetate, an ionic liquid, with a constant flow rate was used in this study to make a conductive fiber and improve characteristics of PEDOT:PSS. Conductive fibers by fibrillary gelation showed enhanced electrical conductivity of about 400 S cm^{-1} and volumetric capacitance of about 154 F cm^{-3} which would be strongly beneficial to be utilized for organic electrochemical transistors (OECTs), resulting in a high transconductance of 19 mS in a depletion-mode. Moreover, dedoping of the conductive fibers by PEI (polyethyleneimine) enabled the creation of enhancement-mode OECTs. Interdigitated inverters were then fabricated by connecting depletion and enhancement-mode OECTs. These results demonstrate that these conductive fibers and electronic-textiles are suitable candidates for applications in bio-integrated electronics.

npj Flexible Electronics (2022)6:31 ; https://doi.org/10.1038/s41528-022-00167-7

INTRODUCTION

Organic electrochemical transistors (OECTs) are composed of a three-electrode system of gate, source, and drain. Unlike conventional organic field-effect transistors (OFETs), OECTs have their own structures in which the electrolyte is in contact with the active channel layer formed between the source and the drain electrodes[1]. The gate voltage changes the flow of ions between the gate/electrolyte interface. As, ions penetrate into the active channel layer, the doping/dedoping state of active channel layer is changed. Due to volumetric gating modulation, OECTs have high volumetric capacitance. They can be operated even in low driving voltage (~1 V). They also have higher transconductance (~mS) than of OFETs (~μS)[2]. Because of these characteristics, OECTs could be strikingly useful for signal amplification. They are being studied promisingly in the class of bioelectronics[3–8].

The most promising conductive polymer used as an active channel layer is poly(3,4-ethylenedioxythiophene):poly(styrene sulfonate) (PEDOT:PSS). PEDOT:PSS is a conjugated polymer that maintains an intrinsically doping state by using PSS as a dopant in PEDOT[9–14]. It has high electrical conductivity and biocompatible properties. It is also stable in an aqueous environment[15–17]. Conventional OECTs with the PEDOT:PSS can operate p-type depletion-mode which has serious demerit on high energy-consumption unlike enhancement-mode FETs. However, among organic materials required to fabricate enhancement-mode OECT[18,19], there is no suitable material that is as highly conductive and water stable as PEDOT:PSS. In addition, it takes too much effort and cost to synthesize materials. Therefore, it is necessary to chemically control the doping state of PEDOT:PSS to change the (bi)polaron state to a neutral state to drive OECTs in an enhancement-mode by effective methods. In addition, most OECTs have liquid electrolyte or are constructed by multi-layers of deposition on a planar substrate such as glass or silicon wafer, making it difficult to be integrated in a textile due to a geometrical mismatch between the substrate and the fabric[20,21]. Therefore, it is inevitable to study a fiber-shaped transistor to use conducting polymers in textile electronics[22]. There have been previous reports PEDOT:PSS fibers with various coagulant such as sulfuric acid[22], acetone[23], DMSO[24] and calcium chloride solutions[25]. However, these are mostly focused on other types of electronic devices like sensors[26,27] and thermoelectric devices[24,25] and fiber-shaped OECTs by using acetone show declined parameters (conductivity, mobility and volumetric capacitance), related to the performance of OECTs[23].

Here, we proposed OECTs of a fiber-type developed with a dedoping process that could be used in textile electronics. Such fiber-type OECTs were composed of microfibers prepared by fibrillary gelation of conductive PEDOT:PSS with biocompatible choline-based ionic liquid (Choline Acetate, [Ch][Ace])[28]. Fibrillary gelation implies molecular alignment of PEDOT:PSS in linear directions, resulting in the formation of dense fibers with constant diameter by physical crosslinking from ionic interaction between PEDOT:PSS and ionic liquids. Such process requires higher concentration of PEDOT:PSS to induce fibrillary gelation with increasing ionic strength[29]. As the ionic liquid ([Ch][Ace]) faces concentrated PEDOT:PSS dispersion through a syringe, it enables to align their molecular structures of PEDOT:PSS and eventually with a transconductance (g_m) of OECTs up to 19 mS, which is higher than previously reported transconductance of fiber-OECTs (g_m = 3.5 mS)[23]. The fibrillary conductive fiber showed a high volumetric capacitance (154 F cm^{-3}). In addition, the operation mode of OECT was controlled by dedoping the conductive fiber using various concentrations of linear PEI and branched PEI[30] operated in enhancement-mode. An integrated circuit was fabricated using two types of PEDOT: PSS fiber, a conductive

[1]School of Chemical Engineering, Sungkyunkwan University (SKKU), Suwon 16419, Republic of Korea. [2]Biomedical Institute for Convergence (BICS), Sungkyunkwan University (SKKU), Suwon 16419, Korea. ✉email: taeilkim@skku.edu

fiber, and a dedoping fiber. The possibility of application to textile electronics capable of signal processing was then suggested.

RESULTS

Fibrillary gelation of conducting polymers

Fibrillary conductive fiber was fabricated by a wet-spinning process. To increase the gelation efficiency of choline-based ionic liquid and PEDOT:PSS, it is better to use viscous dispersion of PEDOT:PSS. Therefore, we used 2.5 wt% PEDOT:PSS (commercialized PEDOT:PSS, Clevios PH1000 with 1.1–1.3 wt%.). It was freeze-dried at −80 °C for a week. It was then dissolved in deionized water (DI) and redispersed by ultrasonication. As shown in Fig. 1a, concentrated PEDOT:PSS solution was injected into choline-based ionic liquid ([Ch][Ace]) at a constant rate (0.1 ml min^{-1}) using a syringe pump to obtain fibrillary gelation of a PEDOT:PSS microfiber. Gelated fibers were placed in [Ch][Ace] ionic liquid overnight, followed by rinsing and annealing processes (middle, see experimental section for details). When 2.5 wt% concentrated PEDOT:PSS dispersion (left) was immerged into the interface with an ionic liquid ([Ch][Ace]), water molecules in the PEDOT:PSS solution were dehydrated in high ionic concentration and excess PSS polymers were dissolved to the ionic liquid, leading to gelation. During the fibrillary gelation, electrostatic interaction between PEDOT and PSS weakens by phase separation and PEDOT main chains are aligned through the injectional direction (right), leading to improved electrical conductivity[31]. In this process, we are able to create fibrillary conductive fiber and control diameters of fibers by using different syringes (Supplementary Fig. 1a–d). We also conducted a dedoping process of fibrillary gelated fibers with PEI (Polyethylenimine). When as-spun fibers were placed in linear PEI and branched PEI overnight before washing and annealing process, PEI molecules entered the fibers and strong amine groups interacted with PSS^-. At this time, PEDOT was chemically reduced and dedoping occurred.

As shown in Fig. 1b, c, PEDOT:PSS injected into DI water (<10^{-6} M) was dispersed by lower ionic strength. Otherwise, through injection to choline based ionic liquid ([Ch][Ace]) (~5 M) with increasing ionic strength, it was confirmed that fibers were created due to fibrillary gelation of PEDOT:PSS. Figure 1d shows mechanical property variation in sol-gel transition of PEDOT:PSS induced by the ionic liquid. It was investigated by plotting storage modulus and loss modulus (tan δ) from dynamic mechanical analysis (DMA). At the injection point, increase of the storage modulus and decrease of the tan δ were found. This was the point at which PEDOT:PSS in sol state changed to PEDOT:PSS in gel state, which could be explained by the fact that when the tan δ had value of 1, the storage modulus and the loss modulus became the same and analyte became solid. Furthermore, we could estimate linear relationship between the diameter of syringes and the conductive fibers, respectively (Supplementary Fig. 1e) and fibers are similar with the thickness of hair, clearly witnessing that they could be used for textile electronics (Fig. 1e, f). Mechanical properties of these fibers were characterized by tensile tests. Results confirmed that when strain was applied to fibrillary conductive fibers at a constant tensile rate of 10 mm min^{-1}, they showed an elongation at break value of 29.5 ± 0.016% and a Young's modulus value of 1.62 ± 0.186 GPa (Supplementary Fig. 2). Mechanical properties of fibrillary conductive fibers are similar with conventional materials and composites in previous reports (Table 1). To verify electrical conductivity against deformation, resistance changes of the fibrillary conductive fiber were measured by bending the fiber in 50% (curvature, r^{-1} = 0.6 mm^{-1}) for 10,000 cycles (Fig. 1g and Supplementary Fig. 2b, c). The trend of ratio (R/R_0) was maintained without significant change even with 10,000 times of bending, although there were some noise signals near the end of cycles, proving the stability of fibrillary conductive fibers.

Morphological analysis of conductive fibers

Results of surface analysis of PEDOT and PSS changes under the influence of gelation by ionic strength are described in Fig. 2. X-ray diffraction (XRD) was carried out to reveal the alignment of PEDOT rod and PSS chain in the fibrillary conductive fiber (blue) and spin-cast PEDOT:PSS (black). As shown in Fig. 2a, it was confirmed that the intensity of the conductive fiber increased at $q = 1.84$ $Å^{-1}$ (d_π-π = 3.4 Å), meaning that the degree of π-π stacking of PEDOT in fibrillary conductive fiber increased compared to that of spin-cast PEDOT:PSS. The molecular packing structure is shown in Fig. 2b, with (010) direction meaning π-π stacking of PEDOT. Also, in the spin-cast PEDOT:PSS, a peak related to π-π stacking of PEDOT appeared as $q = 1.79$ $Å^{-1}$ (d_π-π = 3.49 Å). A slightly reduced π-π stacking distance caused an impressive increase in conductivity due to increasing interchain mobile carrier transport[32]. This also supports why the conductivity of the conductive gel fiber is 400 S cm^{-1}, which is about 1600 times higher than that of a commercial PEDOT:PSS (0.25–0.3 S cm^{-1}).

Figure 2c–e and Supplementary Fig. 3 show topographic and phase of spin-cast PEDOT:PSS film (c and d) and fibrillary conductive fiber (e) images by non-tapping mode of atomic force microscopic (AFM). In the case of PEDOT:PSS film, phase separation between PEDOT core (bright) and PSS-rich region (dark) was not observed[33,34]. However, in the case of the fibrillary conductive fiber and the PEDOT:PSS/PEI fiber, as shown in Figs. 2e and Supplementary Fig. 3b, it was confirmed that the PEDOT core (bright) was obviously agglomerated and aligned molecular structures along the shear direction, compared to those of spin-cast film, even after swelling in ionic liquids, observed both in topography and phase images. We found that PEDOT and PSS phases were separated, and excess PSS was removed. When the pristine PEDOT:PSS film was swollen with choline acetate and PEI, respectively, PEDOT aggregation did not occur significantly (Fig. 2d and Supplementary Fig. 3a). Therefore, it was proved that the alignment between PEDOT and PSS was formed by shear stress during the fibrillary injection.

Electrical/ chemical/ electrochemical characterization of fibrillary conductive fiber

Electrical, chemical, and electrochemical characteristics were evaluated from a series of experiments to utilize fibrillary conductive fibers as a main component in electronic devices as shown in Fig. 3. In the process of dedoping conductive fibers, we immersed fibrillary conductive fibers in PEI solution for penetration into them. The interactions between PEI and other chemical components are shown in Fig. 3a, b. We controlled the amount of dedoping by varying the concentration of linear and branched PEI polymers from 0.001 to 10 g L^{-1}, leading to changes of conductivity as shown in Fig. 3c. Varying the concentration of PEI solution keeping swelling time 12 h showed that swelling in the solution of lower concentration than 0.01 g L^{-1} resulted in dramatic changes of conductivity, while saturation of conductivity was found at higher concentrations. We estimated the range of dedoping by controlling the concentration of PEI solution. From that, irreversible deformation of polythiophene rings in highly concentrated PEI solution (>0.01 g L^{-1}) decreased the performance when fabricated for organic electrochemical transistors. We also characterized electrical properties of fibers by measuring of conductivity in PBS solution for 5 days for applications to bioelectronics (Supplementary Fig. 4). Both fibrillary conductive and dedoped fibers showed as constant electrical conductivity of 464 ± 22.7 S cm^{-1} for conductive and 3.14 ± 0.73 S cm^{-1} for dedoped fibers as the maximum value without noticeable changes in swelling in PBS solution.

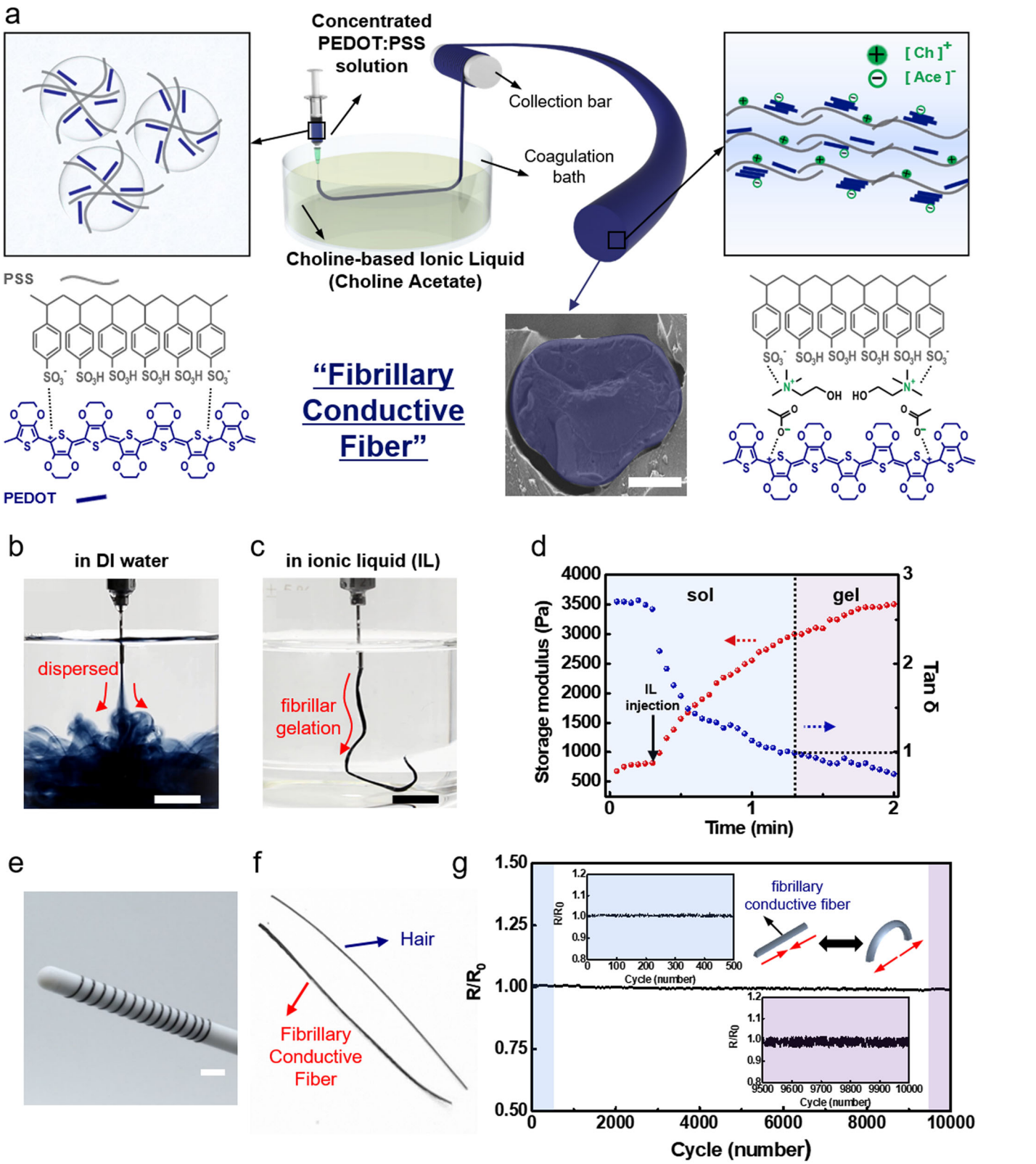

Fig. 1 Fibrillary gelation for a conductive fiber. a Scheme of fabrication of conductive fiber by fibrillary gelation at interface between PEDOT:PSS solution and choline-based ionic liquid, and cross-sectional SEM image of the fiber (highlighted navy, scale bar: 100 μm). Photo images for re-dispersed concentrated PEDOT:PSS solution in DI water (**b**) and fibrillary gelation in choline acetate (**c**), which proves that increasing ionic strength can lead to gelation of PEDOT:PSS (scale bar: 1 cm). **d** Gelation process that occurs by injecting choline-based ionic liquid ([Ch][Ace]) into PEDOT:PSS. When the Tan δ value becomes 1, sol changes to gel. **e** Image of the PEDOT:PSS conductive gel fiber collected on a Teflon bar. **f** Conductive fiber after thermal annealing (scale bar: 1 mm) compared to a human hair. **g** Resistance change (R/R_0) of a single conductive fiber during 10,000 cycles of bending (curvature, $r^{-1} = 0.6\ mm^{-1}$). Insets shows schematic image of bending test and their signal comparisons with initial and final ones.

Table 1. Parameters of conductive fiber and commercial materials for fibers.

References	Materials	Fabrication	Diameter (μm)	Elongation at break (%)	Young's modulus (GPa)
This work	PEDOT:PSS/[Ch][Ace]	Coagulation	100	29.5 ± 0.016	1.62 ± 0.186
[46]	CNT[a]	Twist-spun	100	≈10*	1.62–2.25
[47]	Silk-PEDOT:PSS	Immersion	250	8 ± 1–13 ± 1	1.8 ± 0.3–3.2 ± 0.3
	Cotton-PEDOT:PSS	Immersion	180	6 ± 1–7 ± 1	5.3 ± 0.6–7 ± 2.5
[48]	Cotton-MXene[b]	Dip-coating	610	NA	5.0 ± 0.3
[26]	PA[c]/lycra-PU[d]-PEDOT:PSS	Immersion	–	650–1400	3×10^{-3}–4.5×10^{-3}
[27]	PU-PEDOT:PSS	Wet spinning	80	≈10*	0.01
[49]	Silk-CNT	Coating	60–100	NA[e]	4.3
[50]	Cotton			4–8	5–12
	Wool			25–45	3.2–4.5
	Polyester			>50	13.5

*approximated.
[a]*CNT* Carbon Nano Tube.
[b]*MXene* Ti_3C_2.
[c]*PA* Polyamide.
[d]*PU* Polyurethane.
[e]*NA* Data not available.

X-ray photoelectron spectroscopy (XPS) of pristine PEDOT:PSS, fibrillary conductive fiber, and PEI dedoped fiber was used to confirm chemical interactions between choline based ionic liquid ([Ch][Ace]) and PEI. In the case of dedoped fibers swollen in PEI, the amine group of PEI existed in the form of NH_3^+, and the strong NH_3^+ group of PEI interacted with the sulfonate group of PSS (Fig. 3a, b). As shown in Fig. 3d and Supplementary Fig. 5a, in PEI dedoped fibers, the amine group of PEI was changed from NH_2 to NH_3^+. In addition, both a positively charged nitrogen peak (≈402 eV) and a neutral nitrogen peak (≈400 eV) appeared. For the fibrillary conductive fiber, the amine group of choline acetate ([Ch][Ace]) existed in an ionized state. Thus, only a positively charged nitrogen peak (≈402 eV) appeared. In XPS S 2p spectra, binding energy of 166–172 eV was the sulfonate peak of PSS and 162–166 eV was the thiophene peak of PEDOT (Fig. 3e and Supplementary Fig. 5b)[35]. Under the influence of PEI, as shown in Fig. 3b, PSS^- bound to $PEDOT^+$ in pristine PEDOT:PSS was combined with an amine group. Thus, the binding energy of electrons in sulfur of PSS^- was decreased from 168.5 eV to 167.64 eV[35] (Fig. 3e). Under the influence of the amine group of choline acetate, the sulfur peak of PSS shifted to the right in the fibrillary conductive fiber as well. In addition, the PEDOT peak area to the PSS peak area ratio was decreased in fibrillary conductive fibers and dedoped fibers than in PEDOT:PSS, revealing that excess PSS was removed during fibrillary gelation (Supplementary Fig. 5c)[36].

Raman spectroscopy was performed to confirm the chemical doping state of PEDOT:PSS, the fibrillary conductive fiber, and the dedoped fiber using 785 nm excitation laser source. As shown in Fig. 3f and Supplementary Fig. 6, in the case of fibrillary conductive fiber and dedoped fiber, a peak at 1135 cm^{-1} related to the PSS component and a peak at 1262 cm^{-1} peak related to C_α – C_α′ stretching vibration were decreased significantly compared to those of pristine PEDOT:PSS. It confirmed that the excess PSS was removed by fibrillary gelation of PEDOT:PSS and ionic liquid ([Ch][Ace]). In addition, in the fibrillary conductive fiber to which choline acetate was added and the PEI dedoped fiber, it was be observed that the 1434 cm^{-1} peak corresponding to C_α = C_β stretching vibration became left-shifted, confirming that chemical dedoping occurred from quinoid to benzoid. To confirm the degree of dedoping according to PEI concentration, ultraviolet-visible-near-infrared (UV-VIS-NIR) absorption analysis was performed for pristine PEDOT:PSS, fibrillary conductive gel fiber, and PEI dedoped fibers with various concentrations of PEI (10–0.001 g L^{-1} of Linear PEI). As shown in Fig. 3g, as PEI concentration increased, neutral (~600 nm) and polaron chain absorption intensity (~900 nm) increased while bipolaron chain absorption intensity (~1200 nm) decreased. This trend was similar to the fiber dedoped with branched PEI (Supplementary Fig. 7). It was seen that as PEI concentration increased, the main chemical state of the PEDOT chain changed from bipolaron to polaron and neutral. In addition, it showed good agreement with the decrease in conductivity as the main charge carrier changed to polaron and neutral when PEI concentration increased (Fig. 3c).

In addition to electrical characteristics of fibers, electrochemical impedance spectroscopy (EIS) was conducted to reveal the interaction between PEDOT:PSS and ions in the fiber matrix. Impedance and phase angle were extracted with a three-electrode setup from 10^5 Hz to 0.01 Hz as illustrated in Fig. 3h. In both cases of fibrillary conductive and dedoped fibers, impedance dramatically changed in a lower frequency region (0.01–1 Hz) and maintained at high frequency (>1 Hz), attributed to the formation of capacitor in lower frequency range at the interface between fiber and electrolyte, indicated by phase angle close to −90°[12,37]. In contrast with electric conductivity, we used electrolyte solutions (0.1 M of NaCl) for measurement of impedance to clarify both electronic and ionic conduction at the interface, reflecting the concept of formation of resistors and capacitors[38]. Since it is a result of both conductions, we should evaluate characteristics with various parameters, including volumetric capacitance and current variation by pulsed input voltage, especially for OECTs[39]. Therefore, impedance of conductive and dedoped fibers shows less difference than that of conductivity, because of maintained porosity, although electrical conductivity of fiber is decreased by dedoping. Compared to field-effect transistors, OECTs are based on penetration ions into the channel, facilitating volumetric gating with high capacitance. In terms of volumetric capacitance, higher transconductance can be produced by electrolyte-gated operation with PEDOT:PSS as well-known materials for OECTs. Volumetric capacitance of fibrillary conductive fiber was calculated with raw data from EIS measurement by fitting in an equivalent circuit model, R_s (R_p||C), followed by dividing capacitance with the volume of fiber (Fig. 3i). Fibrillary conductive fibers showed much higher volumetric capacitance of about 154 F cm^{-3} than pristine PEDOT:PSS[40] of about 40 F cm^{-3} attributed to aligned microstructure of the fiber for improved charge distribution and additional charge of ionic liquid in the fiber. By dedoping

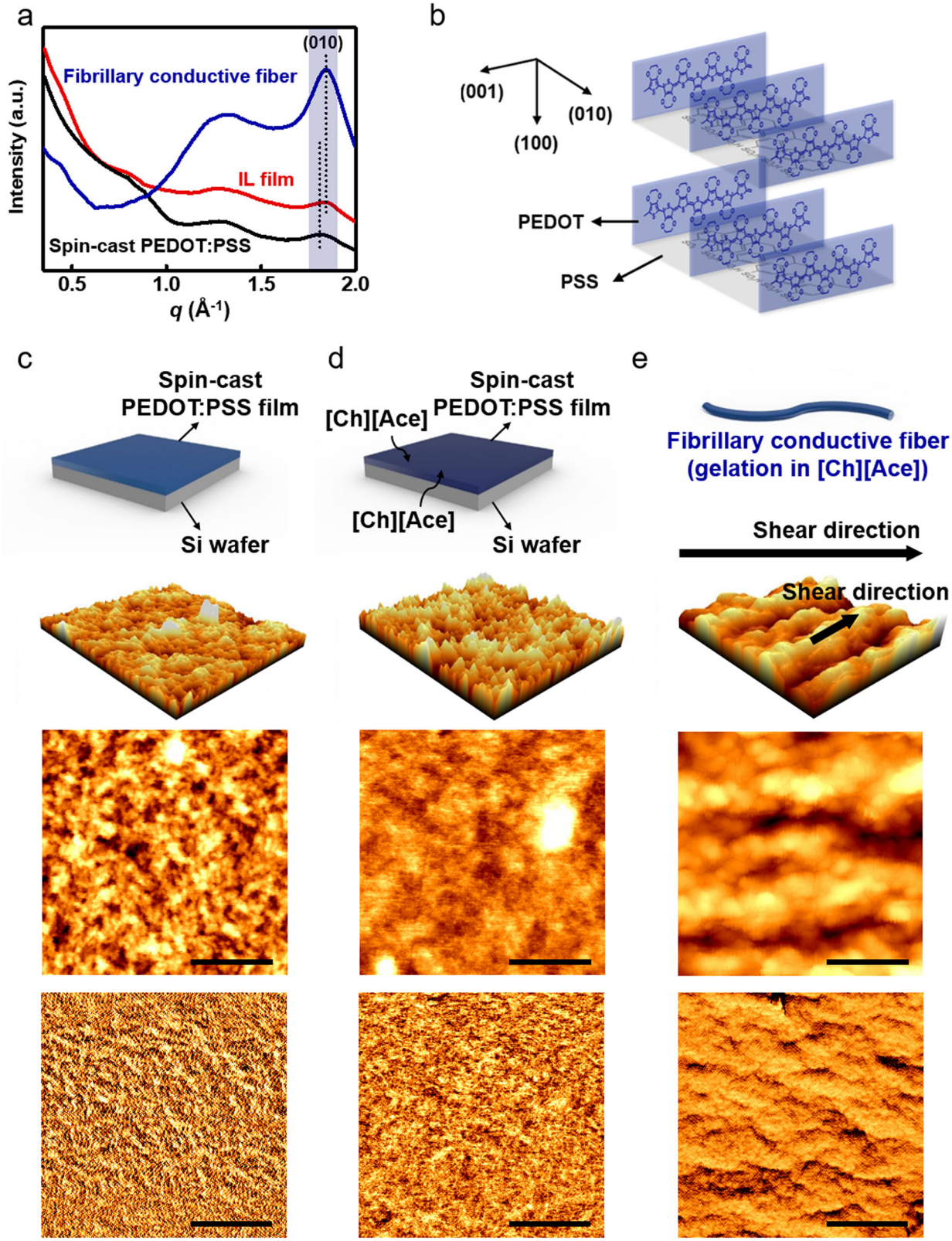

Fig. 2 Morphological characterization of PEDOT:PSS conductive gel fiber. Chemical and surface topological characterization of PEDOT:PSS conductive gel fiber. **a** XRD (TR-WAXD) spectra for spin-cast pristine PEDOT:PSS film (black), PEDOT:PSS film swelled in IL (Red) and fibrillary conductive gel fiber (blue). **b** Schematic diagram for molecular packing structure of semi-crystalline PEDOT:PSS. (010) direction means *π-π* stacking of PEDOT. Surface topologies (Top and middle) and phase (bottom) of PEDOT:PSS by AFM measurement. Spin-cast PEDOT:PSS film for **c**, spin-cast PEDOT:PSS film swelled in choline acetate for **d**, and PEDOT:PSS conductive gel fiber by fibrillary gelation with choline acetate for **e**. (all scale bars show 0.5 μm).

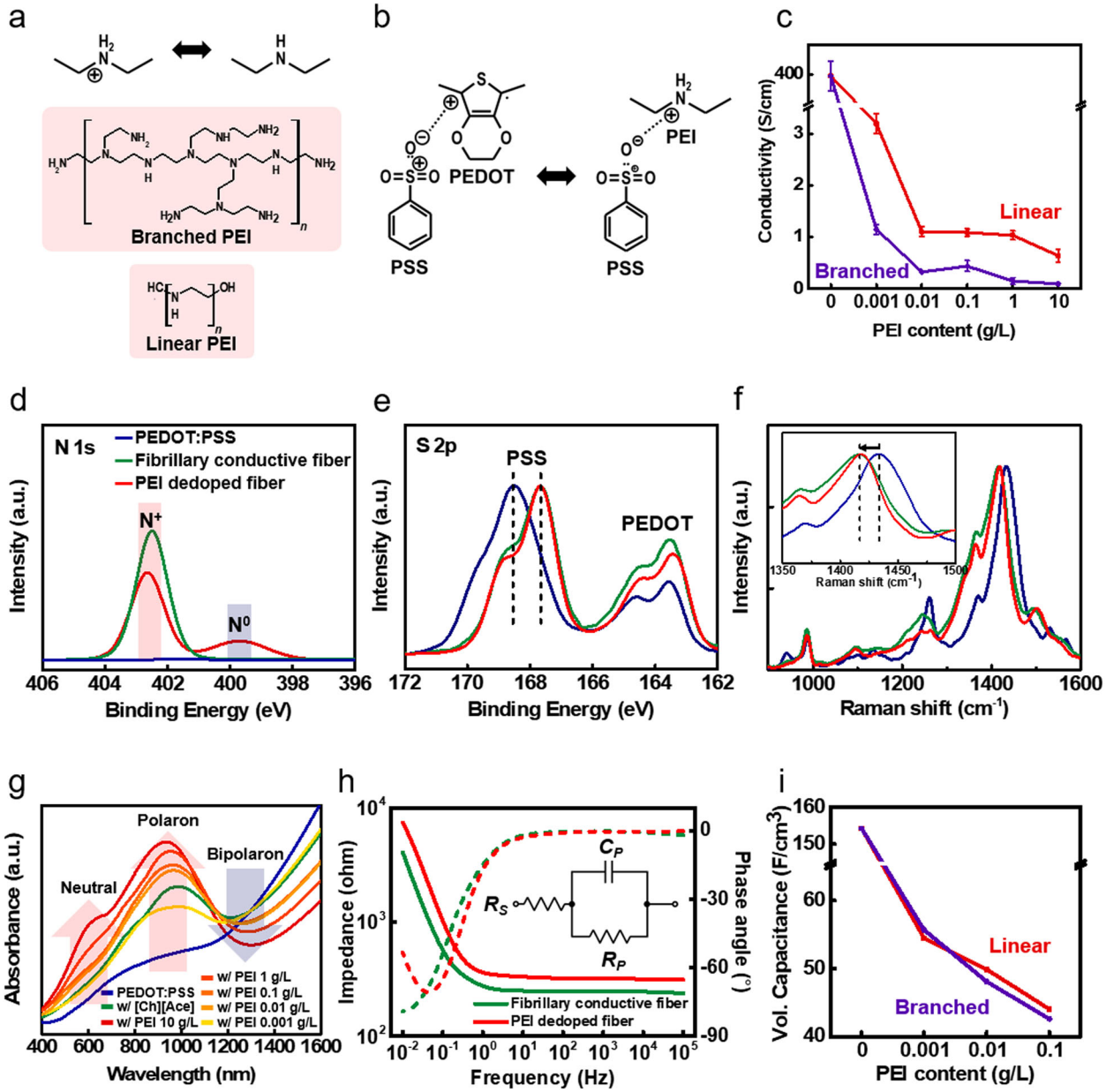

Fig. 3 Electrical, chemical, and electrochemical properties of the PEDOT:PSS conductive gel fiber. a, **b** Schematic diagram showing the state of interaction of nitrogen and sulfur, respectively. **c** Conductivity of the PEDOT:PSS conductive gel fiber with respect to concentration of linear and branched PEI solution where fibers are swelled for dedoping process. The error bar is about ±10% **d** N 1 s XPS spectra, **e** S 2p XPS spectra, **f** Raman spectra for PEDOT:PSS surface, PEDOT:PSS conductive gel fiber by ionic liquid (PEDOT:PSS/choline acetate) and dedoped fiber by PEI using a 785 nm excitation laser source. **g** UV-vis-NIR spectra for pristine PEDOT:PSS (blue) and [Ch][Ace] (green), PEI addition, respectively. The higher the PEI concentration (Red), the higher the neutral (~600 nm) and polaron (~900 nm) peaks tend to increase. **h** Impedance (solid) and phase angle (dash) of fibrillary conductive fiber and dedoped fiber as a function of frequency. **i** Volumetric capacitance of conductive fibers with respect to concentration of PEI solution.

conductive fibers, charge compensation of PEDOT:PSS by PEI chains caused a decrease of volumetric capacitance as a function of the concentration of PEI solution.

Organic electrochemical transistors based on fibrillary conductive fiber

We investigated characteristics of fibrillary conductive fiber-based organic electrochemical transistor to correlate electrical and electrochemical properties and performances of OECTs. As shown in Fig. 4a, we constructed fiber-based OECTs by crossing two individual fibers and connecting with gelatin hydrogel for gating[41] in pre-patterned PDMS molds, followed by definition of channel on conductive fiber with photo-curable polymer to prevent leakage current (Supplementary Fig. 8a). We can control the channel geometry by partial curing and channel opening with photomask (Supplementary Fig. 8b). To validate the change of operation mode in OECTs, we utilized conductive and dedoped fibers to fabrication of transistors with an identical geometry (200 μm of width and 2 mm of length). In depletion-mode of OECTs, we applied a drain-source voltage from 0 V to −0.8 V with a gate voltage from 0 V to 0.8 V in 0.1 V steps for output characteristics (Fig. 4b) and a gate voltage sweep from 0 V to 0.8 V at −0.6 V of drain-source voltage for transfer characteristics (Fig. 4c). Fibrillary conductive fiber showed 19 mS at V_GS = 0.1 V from

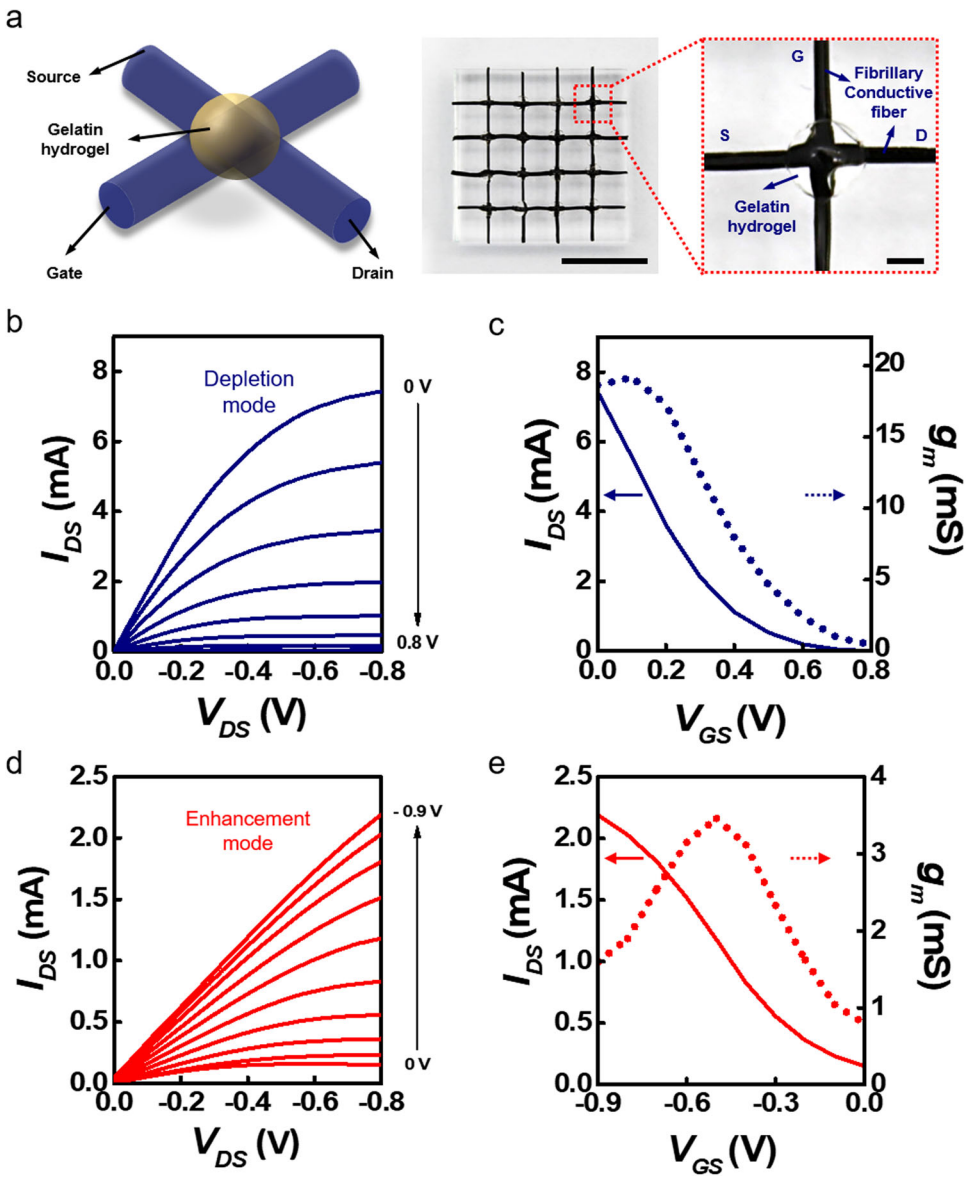

Fig. 4 PEDOT:PSS conductive fibers based interdigitated organic electrochemical transistors. a Schematic illustration and photographs of PEDOT:PSS conductive gel fiber-based OECTs (scale bar = 1 cm). **b**–**e** Characteristics of organic electrochemical transistors (OECTs) with PEDOT:PSS conductive gel fiber. (Width of 200 μm and Length of 2 mm). **b** Output and **c** transfer (at V_DS = −0.6 V) characteristics of PEDOT:PSS conductive gel fibers based OECTs operated in a depletion-mode. **d** Output and **e** transfer (at V_DS = −0.6 V) characteristics of PEDOT:PSS conductive gel fiber with PEDOT:PSS/PEI-based OECTs in an enhancement-mode.

electrical characteristics which was much higher than those of previous reported data with fiber-shaped OECTs[22,23,42]. This was ascribed to aligned PEDOT:PSS chains and existence of choline acetate as an ionic additive in the fiber. We also estimated the effect of ratio between gate and channel area. As previously reported[43], the larger area of gate electrode than the channel is ascribed to higher on/off current ratio and transconductance, as shown in Supplementary Fig. 9. In case of enhancement-mode operated OECTs with dedoped fibers, negative gate voltage was applied to measure characteristics of devices from 0 V to −0.9 V in −0.1 V intervals with drain-source voltage from 0 V to −0.8 V for output characteristics (Fig. 4d) and gate voltage was swept from 0 V to −0.9 V at V_DS = −0.6 V (Fig. 4e) of drain-source voltage for transfer characteristics. Compared to the performance of depletion-mode OECTs, we acquired an increase of current by negative gate voltage from 0.15 mA to 2.1 mA and 3.4 mS of maximum transconductance at V_GS = −0.5 V. Values of maximum current and transconductance of enhancement-mode were lower than those of depletion-mode, due to the decrease of conductivity and volumetric capacitance by PEI-based dedoping of PEDOT:PSS. These characteristics are dependent on the concentration of linear and branched PEI solutions as shown in Supplementary Fig. 10. As mentioned, irreversible deformation of polythiophene rings in PEDOT main chains leads to the decline of current level and transconductance.

The charge transport characteristic of OECTs was investigated because the active layer caused volumetric response, compared with organic field-effect transistors (OFETs). Therefore, we plotted the relationship between transconductance(g_m) and $W\ D\ L^{-1}$ (V_th-V_G) by examining the channel width (W), channel depth (D), and channel length (L) from transfer curves of several devices with various channel geometries. As shown in Supplementary Fig. 11, we acquired a plot with linearity (slope is $\mu C^* = 455.75\ \mathrm{F\ cm^{-1}\ V^{-1}\ s^{-1}}$), which had a good agreement with benchmarking of Inal

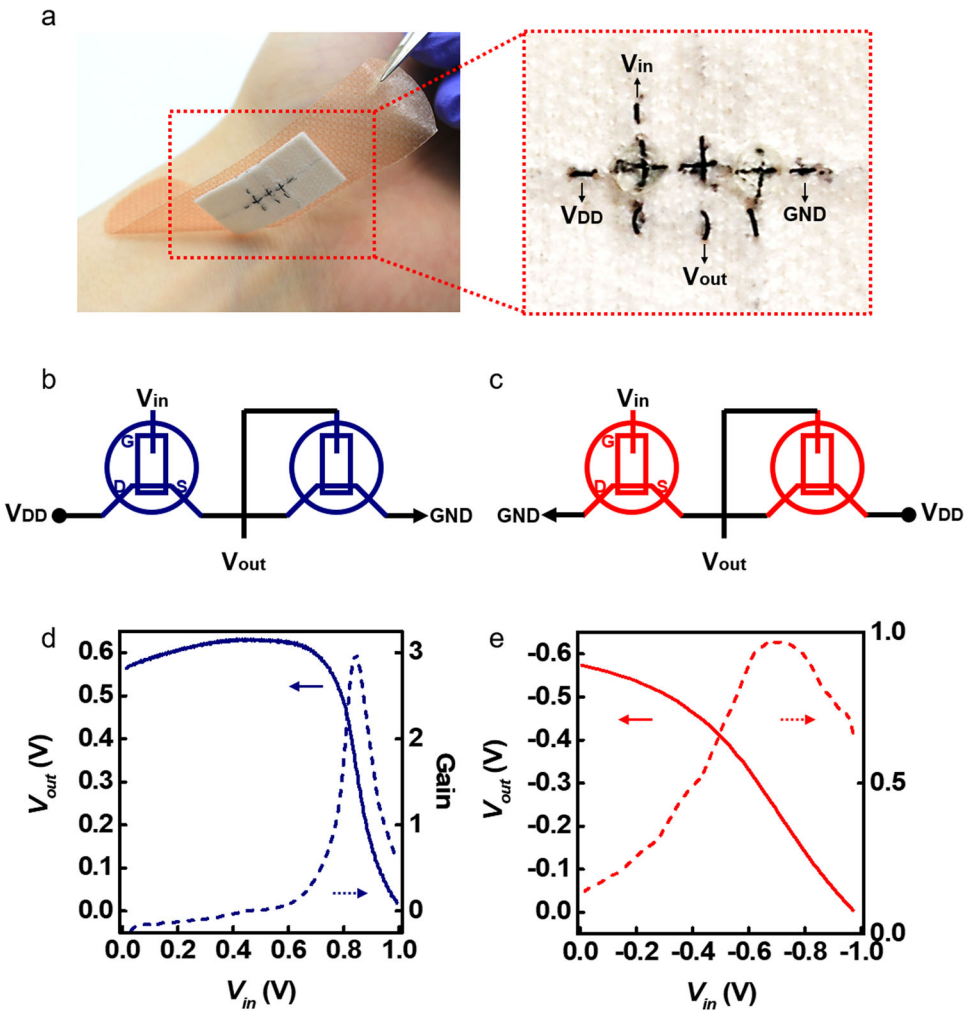

Fig. 5 Inverters composed of interdigitated OECT with PEDOT:PSS conductive gel fiber. a Integrated circuit of zero-V_{GS} implemented by suturing in a plaster. Equivalent circuits of **b** depletion-mode OECTs based and **c** enhancement-mode OECTs based inverters. **d**, **e** Corresponding transfer characteristics of inverters (navy: depletion-mode OECTs based inverter, red: enhancement-mode OECTs based inverter) at $|V\_DD| = 0.6$ V.

et al.[44]. Based on 154 F cm^{-3}, we estimated the mobility of fiber-OECTs as 2.96 cm^2 V^{-1} s^{-1}. It means that fibrillary gelation of PEDOT:PSS leads to improved performance of OECTs, compared to pristine PEDOT:PSS based OECTs[14]. To evaluate durability and reliability under deformation, we characterized the performance when fiber-OECTs are stretched by 30% (Supplementary Fig. 12). Due to stretchability of the fibers in previous section, the performance of fiber-OECTs indicated with on/off ratio and maximum transconductance is maintained, even under 30% and repeated stretching to 100 cycles. We also characterize responses of both depletion and enhancement mode fiber-OECTs by pulse with 1 Hz on gate electrode (Supplementary Fig. 13). In the responses, we observed sharp peaks at the switching moments which are ascribed to the polarization/depolarization of the electrolyte in the operation of fiber-OECTs and insufficient times to escape for injected ions[45]. The current changes for 2 h in fiber-OECTs are constant and response times are also around 200 ms, regardless of operation modes.

Integrated circuits with OECTs based on fibrillary conductive fiber

We fabricated fiber OECT-based inverter circuits to further demonstrate the application of fibrillary conductive fibers. We successfully integrated inverters fabricated with conductive fibers in the fabric of a sticking plaster by suturing in designed directions (Fig. 5a). As shown in Fig. 5b, c, we designed inverter circuits for depletion-mode and enhancement-mode OECTs. Inverters were fabricated by defining driving and load parts by casting gelatin hydrogels on two different points in a single fiber. For inverters with depletion-mode OECTs, the ground was connected to a source electrode of loaded OECT (Fig. 5c). In case of enhancement-mode OECTs, the ground was connected to a source electrode of driving OECT. To evaluate characteristics of two inverters, we swept gate voltage from 0 V to ±1 V with ±1.5 V of drain voltage (positive: depletion-mode (Fig. 5d) and negative: enhancement-mode (Fig. 5e)). Each transfer characteristic was then demonstrated. In depletion-mode inverters, output voltage was 19 mV as '0' signal by 1.0 V of the input voltage and close to 0.56 V as '1' signal by 0 V as the input voltage, with 3 of maximum gain (ΔV_out/ΔV_in) at 0.84 V input. Otherwise, in case of enhancement-mode inverters, output was −0.57 V by 0 V of input voltage and 4.7 mV by −1 V of input voltage with 1 of maximum gain at −0.7 V of input voltage. The reason why the value of maximum gain in enhancement-mode inverters was lower than that of depletion-mode in range of demonstrating each transistor as described in previous sections was ascribed to the decline of conductivity by dedoping of PEDOT:PSS. Moreover, each inverter showed an opposite direction of driving, depending on the

operation mode of OECTs. Both inverters successfully produced converted output signals, corresponding to input signals, demonstrating a huge potential of application to bioelectronics as a main component in signal processing.

DISCUSSION

We demonstrated fibrillary gelation of conducting polymer, PEDOT:PSS, by injection to biocompatible and biodegradable ionic liquid, choline acetate with applying shear forces that induced molecular arrangement. Conductive fibers have application as high-performance organic electrochemical transistors and integrated circuits. A comprehensive series of experimental results and analysis of data for studying physical and electrical/electrochemical properties enabled us to explore the relationship in these materials. Well-aligned molecular structures and addition of ionic liquid in fibrillary conductive fibers yield improved characteristics, such as electric/ionic conductivity and volumetric capacitance of electronics devices, especially for OECTs with hydrogels. Furthermore, controlling operation mode of OECTs in depletion and enhancement-mode by selective dedoping of conductive fibers can fabricate of integrated circuits for signal processing, including filtering and amplifying devices based on OECTs for biological and biochemical signals of living organisms. We believe that this work demonstrates many opportunities where biocompatible materials and high aspect ratio of conductive fibers can contribute to the creation of advanced e-textile in stimulating and monitoring devices, with applications to wearable and implantable electronics for biomedical fields.

METHODS

Preparation of fibrillary gelation of conductive fibers

PEDOT:PSS dispersion (Clevios PH1000, Heraeus Holding GmbH, Germany) was freeze-dried at −80 °C for 7 days. Solid PEDOT:PSS was re-dispersed in deionized water (DI water) to make concentrated dispersion (2.5 wt%) mixed with polyethylene glycol (M_w = 2,000,000), ethylene glycol (5%, v v^{-1}), 4-dodecylbenzenesulfonic acid (0.1% w v^{-1}) (Sigma-Aldrich, Saint Louis, MO, USA) and (3-glycidyloxypropyl)trimethoxysilane (1%, w v^{-1}). After ultrasonication, concentrated PEDOT:PSS dispersion was injected into choline-acetate ionic liquid with a constant flow of 0.1 ml min^{-1} using a syringe pump (NE-300, KF Technology) and 21 G needles after filtering through 0.45 μm of PTFE syringe filters. For ionic liquid with 5 M ionic strength, choline bicarbonate (Sigma-Aldrich, Saint Louis, MO, USA) and acetic acid (Samchun Chemical, Korea) were reacted at 1:1 mole ratio. the ionic liquid was purified by removing carbon dioxide and water in a vacuum chamber. The fiber was placed in bath containing ionic liquid ([Ch][Ace]) overnight, washed with DI water and annealed at 150 °C for one hour to make fibrillary gelation of conductive fiber. Linear (M_n = 2100) and branched (M_w = 25,000)-polyethyleneimine (PEI, Sigma-Aldrich) dissolved in [Ch][Ace]/water (50%, w w^{-1}) were used. For fabricating dedoping fibers, fibers were placed in linear PEI or branched PEI chamber at various concentrations (10 g L^{-1}–0.001 g L−1) in a vacuum chamber overnight, followed by washing and annealing processes as described above.

XRD measurement

XRD analysis was conducted by X-ray Diffraction (D8 DISCOVER, Bruker) with 4–39 degrees of 2 theta by transmission mode. All fiber samples were directly loaded on the sample holder aligned in the same direction.

AFM measurement

AFM images and 3D morphology images were obtained with Atomic Force Microscopes (XE150, PSIA) in non-tapping mode. Fibrillar conductive fibers including PEDOT:PSS/PEI fibers were directly attached onto double-sided carbon tape. All images were acquired at 1.5 μm × 1.5 μm and flattering to remove topology variations.

XPS measurement

XPS measurement was carried out with k_α X-ray Photoelectron Spectroscopy (NEXSA, Thermo Fisher Scientific). All samples were prepared with powder type of the fiber using a grinder. Spectra peaks were deconvoluted with Spectra Data Processor (SDP) v8.0.

Raman spectroscopy

Raman spectra were measured by Raman spectroscopy (alpha 300, WiTec) with a 532 nm excitation laser source and a scanning wavenumber of 700–1800 cm^{-1}. All fiber samples were prepared by fixing both ends with polyimide (PI) tape on a glass substrate.

UV-vis-NIR spectroscopy

UV-vis-NIR absorption spectra were acquired by ultraviolet-visible-near-infrared spectroscopy (Cary 5000, Agilent Technologies, USA) with 300–1800 nm in 1 nm increment. Pristine PEDOT:PSS was spin-coated on a glass substrate. Fibrillary conductive fibers and PEI dedoped fibers were loaded on a glass substrate in abundance.

Mechanical and electrical/electrochemical characterization of the fibrillary gelation of conductive fibers

Mechanical properties of fibrillary gelation of conductive fibers were characterized with a universal tensile machine (UTM, 3342, Instron Co.). These fibers were stretched in constant rate (10 mm min^{-1}). moduli of fibers were calculated with the value from average of samples. The durability test was conducted by performing 50% bending of the fiber (length = 5 cm) 10,000 times at a speed of 3 s/cycle.

Impedance of the fiber was measured with a Potentiostat (ZIVE SP2, WonATech, Korea) by applying 25 mV of AC voltage in a range of frequency from 10^5 to 0.01 Hz. The fiber (as a working electrode) was connected to a platinum (Pt) counter electrode and a Ag/AgCl reference electrode. Electrochemical characterization was done in a 0.1 M of sodium chloride (NaCl, Samchun Chemical, Korea) solution with these three electrodes.

Conductivity (σ) values of fibers were calculated with values of resistance (R) by TLM (Transfer Length Method). Fibrillary conductive fibers were connected to gold electrodes patterned by photolithography with various channel lengths (10, 25, 50, 100, 250, and 500 μm). Resistance of fibers in each channel length was measured with a semiconductor parameter analyzer (B1500A, Agilent, USA). Cross-sectional area (A) of the fiber was calculated with ImageJ program (version 1.52p) using images of optical microscopy (Leica DM2700M, Leica Microsystems Inc.) The length (l) of the fiber was measured with vernier calipers. The conductivity was then calculated with the following equation:

$$\sigma = l\, R^{-1} A^{-1} \quad (1)$$

Stability test was performed by measuring the change in conductivity after soaking the fiber in PBS (0.1 M, pH 7.4) solution for 12, 24, 36, 48 h up to 120 h.

Fabrication of OECTs and integrated circuits using the conductive fiber

To define channel geometry, precursor for the photo-curable polymer (polyurethane acrylate, CFM−110s, MCNet, Korea) was placed on conductive fibers. Fibers were then aligned with a photomask having patterns for OECTs and integrated circuits. After alignment, polymer was pre-cured by UV in a short time (17 mW cm^{-2}, ~2 s) and residual was washed with IPA (isopropylalcohol). For full curing, samples were subjected to UV flood exposure (MT-UV-A31, Minuta Tech, Korea) at 0.2 mW cm^{-2} overnight. Gelatin (Type A, Sigma-Aldrich, Saint Louis, MO, USA) hydrogel as an electrolyte was then cast on the channel of OECTs and integrated circuits.

Characterization of OECTs and integrated circuits with the conductive fibers

Electrical characteristics of conductive fibers based OECTs were determined with a semiconductor parameter analyzer (B1500A, Keysight Technology, USA). For transfer characteristics, gate-source voltage (V_GS) and drain-source voltage (V_DS) were applied to each terminal according to the operation mode of OECTs. Characterization of integrated circuits

was done with a DC voltage supplier (B2912A, Keysight Technology, USA) and an oscilloscope (DSOX2014A, Keysight Technology, USA). Input voltage was applied to the gate electrode of driving OECTs. Output electrodes of circuits were then connected to an oscilloscope. Transfer curves were recorded in a constant period.

DATA AVAILABILITY

The data that support the finding of this study are available from the corresponding author upon reasonable request.

Received: 6 December 2021; Accepted: 10 May 2022;
Published online: 26 May 2022

REFERENCES

1. Khodagholy, D. et al. In vivo recordings of brain activity using organic transistors. *Nat. Comm.* **4**, 1575 (2013).
2. Rivnay, J. et al. Organic electrochemical transistors. *Nat. Rev. Mater.* **3**, 17086 (2018).
3. Lee, W. et al. Transparent, conformable, active multielectrode array using organic electrochemical transistors. *Proc. Natl Acad. Sci. USA* **114**, 10554–10559 (2017).
4. Park, S. et al. Self-powered ultra-flexible electronics via nano-grating-patterned organic photovoltaics. *Nature* **561**, 516–521 (2018).
5. Lee, H. et al. Ultrathin Organic Electrochemical Transistor with Nonvolatile and Thin Gel Electrolyte for Long-Term Electrophysiological Monitoring. *Adv. Funct. Mater.* **29**, 1906982 (2019).
6. Cicoira, F. et al. Influence of Device Geometry on Sensor Characteristics of Planar Organic Electrochemical Transistors. *Adv. Mater.* **22**, 1012–1016 (2010).
7. Romele, P. et al. Multiscale real time and high sensitivity ion detection with complementary organic electrochemical transistors amplifier. *Nat. Comm.* **11**, 3743 (2020).
8. Romele, P., Ghittorelli, M., Kovács-Vajna, Z. M. & Torricelli, F. Ion buffering and interface charge enable high performance electronics with organic electrochemical transistors. *Nat. Comm.* **10**, 3044 (2019).
9. Xu, J. et al. Highly stretchable polymer semiconductor films through the nanoconfinement effect. *Science* **355**, 59–64 (2017).
10. Rivnay, J., Owens, R. M. & Malliaras, G. G. The Rise of Organic Bioelectronics. *Chem. Mater.* **26**, 679–685 (2014).
11. Palumbiny, C. M. et al. The Crystallization of PEDOT:PSS Polymeric Electrodes Probed In Situ during Printing. *Adv. Mater.* **27**, 3391–3397 (2015).
12. Kim, S.-M. et al. Influence of PEDOT:PSS crystallinity and composition on electrochemical transistor performance and long-term stability. *Nat. Comm.* **9**, 3858 (2018).
13. Zeglio, E. & Inganäs, O. Active Materials for Organic Electrochemical Transistors. *Adv. Mater.* **30**, 1800941 (2018).
14. Rivnay, J. et al. Structural control of mixed ionic and electronic transport in conducting polymers. *Nat. Comm.* **7**, 11287 (2016).
15. Yuk, H. et al. 3D printing of conducting polymers. *Nat. Comm.* **11**, 1604 (2020).
16. Feig, V. R., Tran, H., Lee, M. & Bao, Z. Mechanically tunable conductive interpenetrating network hydrogels that mimic the elastic moduli of biological tissue. *Nat. Comm.* **9**, 2740 (2018).
17. Volkov, A. V. et al. Understanding the Capacitance of PEDOT:PSS. *Adv. Funct. Mater.* **27**, 1700329 (2017).
18. Yang, C.-Y. et al. A high-conductivity n-type polymeric ink for printed electronics. *Nat. Comm.* **12**, 2354 (2021).
19. Cea, C. et al. Enhancement-mode ion-based transistor as a comprehensive interface and real-time processing unit for in vivo electrophysiology. *Nat. Mater.* **19**, 679–686 (2020).
20. Tian, X. et al. Wireless body sensor networks based on metamaterial textiles. *Nat. Electron.* **2**, 243–251 (2019).
21. Gualandi, I. et al. Textile Organic Electrochemical Transistors as a Platform for Wearable Biosensors. *Sci. Rep.* **6**, 33637 (2016).
22. Kim, Y. et al. Organic electrochemical transistor-based channel dimension-independent single-strand wearable sweat sensors. *NPG Asia Mater.* **10**, 1086–1095 (2018).
23. Kim, Y. et al. Strain-Engineering Induced Anisotropic Crystallite Orientation and Maximized Carrier Mobility for High-Performance Microfiber-Based Organic Bioelectronic Devices. *Adv. Mater.* **33**, 2007550 (2021).
24. Sarabia-Riquelme, R., Shahi, M., Brill, J. W. & Weisenberger, M. C. Effect of Drawing on the Electrical, Thermoelectrical, and Mechanical Properties of Wet-Spun PEDOT:PSS Fibers. *ACS Appl. Polym. Mater.* **1**, 2157–2167 (2019).
25. Yuan, D. et al. Twisted yarns for fiber-shaped supercapacitors based on wetspun PEDOT:PSS fibers from aqueous coagulation. *J. Mater. Chem. A* **4**, 11616–11624 (2016).
26. Tadesse, M. G. et al. Electrically conductive highly elastic polyamide/lycra fabric treated with PEDOT:PSS and polyurethane. *J. Mater. Sci.* **54**, 9591–9602 (2019).
27. Seyedin, M. Z., Razal, J. M., Innis, P. C. & Wallace, G. G. Strain-Responsive Polyurethane/PEDOT:PSS Elastomeric Composite Fibers with High Electrical Conductivity. *Adv. Funct. Mater.* **24**, 2957–2966 (2014).
28. Jo, Y. J. et al. Biocompatible and Biodegradable Organic Transistors Using a Solid-State Electrolyte Incorporated with Choline-Based Ionic Liquid and Polysaccharide. *Adv. Funct. Mater.* **30**, 1909707 (2020).
29. Leaf, M. A. & Muthukumar, M. Electrostatic Effect on the Solution Structure and Dynamics of PEDOT:PSS. *Macromolecules* **49**, 4286–4294 (2016).
30. van der Pol, T. P. A. et al. The Mechanism of Dedoping PEDOT:PSS by Aliphatic Polyamines. *J. Phys. Chem. C.* **123**, 24328–24337 (2019).
31. Wang, Y. et al. A highly stretchable, transparent, and conductive polymer. *Sci. Adv.* **3**, e1602076 (2017).
32. Hosseini, E., Ozhukil Kollath, V. & Karan, K. The key mechanism of conductivity in PEDOT:PSS thin films exposed by anomalous conduction behaviour upon solvent-doping and sulfuric acid post-treatment. *J. Mater. Chem. C.* **8**, 3982–3990 (2020).
33. Xu, B. et al. Functional solid additive modified PEDOT:PSS as an anode buffer layer for enhanced photovoltaic performance and stability in polymer solar cells. *Sci. Rep.* **7**, 45079 (2017).
34. Lu, B. et al. Pure PEDOT:PSS hydrogels. *Nat. Comm.* **10**, 1043 (2019).
35. van de Burgt, Y. et al. A non-volatile organic electrochemical device as a low-voltage artificial synapse for neuromorphic computing. *Nat. Mater.* **16**, 414–418 (2017).
36. Mengistie, D. A., Ibrahem, M. A., Wang, P.-C. & Chu, C.-W. Highly Conductive PEDOT:PSS Treated with Formic Acid for ITO-Free Polymer Solar Cells. *ACS Appl. Mater. Interfaces* **6**, 2292–2299 (2014).
37. Stavrinidou, E., Sessolo, M., Winther-Jensen, B., Sanaur, S. & Malliaras, G. G. A physical interpretation of impedance at conducting polymer/electrolyte junctions. *AIP Adv.* **4**, 017127 (2014).
38. Proctor, C. M., Rivnay, J. & Malliaras, G. G. Understanding volumetric capacitance in conducting polymers. *J. Polym. Sci. B Polym. Phys.* **54**, 1433–1436 (2016).
39. Liu, Y. et al. Soft and elastic hydrogel-based microelectronics for localized low-voltage neuromodulation. *Nat. Biomed. Eng.* **3**, 58–68 (2019).
40. Rivnay, J. et al. High-performance transistors for bioelectronics through tuning of channel thickness. *Sci. Adv.* **1**, e1400251 (2015).
41. Jo, Y. J., Kwon, K. Y., Khan, Z. U., Crispin, X. & Kim, T.-I. Gelatin Hydrogel-Based Organic Electrochemical Transistors and Their Integrated Logic Circuits. *ACS Appl. Mater. Interfaces* **10**, 39083–39090 (2018).
42. Tarabella, G. et al. A single cotton fiber organic electrochemical transistor for liquid electrolyte saline sensing. *J. Mater. Chem.* **22**, 23830–23834 (2012).
43. Koutsouras, D. A., Torricelli, F., Gkoupidenis, P. & Blom, P. W. M. Efficient Gating of Organic Electrochemical Transistors with In-Plane Gate Electrodes. *Adv. Mater. Technol.* **6**, 2100732 (2021).
44. Inal, S., Malliaras, G. G. & Rivnay, J. Benchmarking organic mixed conductors for transistors. *Nat. Comm.* **8**, 1767 (2017).
45. Gkoupidenis, P., Schaefer, N., Garlan, B. & Malliaras, G. G. Neuromorphic Functions in PEDOT:PSS Organic Electrochemical Transistors. *Adv. Mater.* **27**, 7176–7180 (2015).
46. Kim, J.-G., Suh, D. & Kang, H. Large variation in Young's modulus of carbon nanotube yarns with different diameters. *Curr. Appl. Phys.* **21**, 96–100 (2021).
47. Ryan, J. D., Mengistie, D. A., Gabrielsson, R., Lund, A. & Müller, C. Machine-Washable PEDOT:PSS Dyed Silk Yarns for Electronic Textiles. *ACS Appl. Mater. Interfaces* **9**, 9045–9050 (2017).
48. Uzun, S. et al. Knittable and Washable Multifunctional MXene-Coated Cellulose Yarns. *Adv. Funct. Mater.* **29**, 1905015 (2019).
49. Ye, C. et al. Design and Fabrication of Silk Templated Electronic Yarns and Applications in Multifunctional Textiles. *Matter* **1**, 1411–1425 (2019).
50. Elmogahzy, Y., Farag, R. in *Handbook of Properties of Textile and Technical Fibres* (*Second Edition*) (ed Anthony R. Bunsell) 223-273 (Woodhead Publishing, 2018).

ACKNOWLEDGEMENTS

The authors would like to thank Jong Uk Kim for helpful discussions concerning the devices. This research was supported by the National Research Foundation (NRF) funded by the Korean government (MSIT) (NRF-2018M3A7B4071110, and NRF-2020M3C1B8016137).

AUTHOR CONTRIBUTIONS

Y.J.J. and S.Y.K. contributed equally to this work. Y.J.J. and S.Y.K. wrote the manuscript under supervision of T. –i.K. and conceived the original idea, designed the research and conducted experiment and analysis. J.H.H. contributed to fabrication and measurement of samples. B.P. contributed to design of experimental tools and S.C. contributed to chemical analysis. G.R.K. contributed to design of transistor devices and circuits.

COMPETING INTERESTS

The authors declare no competing interests.

ADDITIONAL INFORMATION

Supplementary information The online version contains supplementary material available at https://doi.org/10.1038/s41528-022-00167-7.

Correspondence and requests for materials should be addressed to Tae-il Kim.

Reprints and permission information is available at http://www.nature.com/reprints

Publisher's note Springer Nature remains neutral with regard to jurisdictional claims in published maps and institutional affiliations.